Available online at www.sciencedirect.com
ScienceDirect
Journal of Sound and Vibration 325 (2009) 321–337
JOURNAL OF SOUND AND VIBRATION
www.elsevier.com/locate/jsvi

Elasto-plastic and geometrically nonlinear vibrations of beams by the *p*-version finite element method

P. Ribeiro[a,*], G.H.M. van der Heijden[b]

[a]*DEMEGI/IDMEC, Faculdade de Engenharia, Universidade do Porto, R. Dr. Roberto Frias, s/n, 4200-465 Porto, Portugal*
[b]*Centre for Nonlinear Dynamics, University College London, Gower Street, London WC1E 6BT, UK*

Received 17 November 2008; received in revised form 2 March 2009; accepted 6 March 2009
Handling Editor: M.P. Cartmell
Available online 5 April 2009

Abstract

A model based on a Timoshenko beam *p*-version finite element is developed to analyse oscillations that are, simultaneously, elasto-plastic and geometrically nonlinear. The geometrical nonlinearity is represented by Von Kármán type strain–displacement relations and the stress–strain relation is of the bilinear type, with mixed strain hardening. The equations of motion are obtained using the principle of virtual work and are solved in the time domain by an implicit Newmark method. The Von Mises yield criterion is employed and the flow theory of plasticity applied; if plastic flow is found at a point of the domain, the total plastic strain is determined by summation. Numerical examples are carried out in order to demonstrate that the *p*-version element here advocated has a number of advantages and to show the influence of the plastic and geometrically nonlinear terms on the oscillations of beams.

1. Introduction

Large amplitude nonlinear vibrations, which cause large strains and stresses, are an important problem in many structures including beams. Their study requires geometrically nonlinear models [1–4]. On the other hand, at stresses where Hooke's law is no longer valid it becomes necessary to consider the inelastic behaviour of materials. Unlike elastic deformation, plastic deformation is not a reversible process and depends on the loading path, making structural analysis more complex [5,6].

Some aspects of the vibrations of beams with elasto-plastic behaviour have been analysed before; a brief review is provided in the following lines, in chronological order. In Ref. [7] the response of a beam, where moderate plastic straining occurs due to a short pulse of transverse loading, is investigated. A simple two-degree-of-freedom (dof) model based on a Shanley-type approach is used to represent the beam. In this model a beam is approximated by rigid links joined by a linear elastic–perfectly plastic element; it is additionally considered that the yield stress in tension and compression are equal. With these approximations, Shanley-type models simplify the continuous elasto-plastic beam problem, reducing the system to a low-dimensional

*Corresponding author. Tel.: +351 22 508 17 21; fax: +351 22 508 14 45.
E-mail address: pmleal@fe.up.pt (P. Ribeiro).

0022-460X/$ - see front matter © 2009 Elsevier Ltd. All rights reserved.
doi:10.1016/j.jsv.2009.03.009

discrete one. The existence of chaos is proved in Ref. [7] by computing the Lyapunov exponents. Manoach and Karagiozova [8] analysed the influence of transverse shear on the response of a thick elasto-plastic beam subjected to impulse loads. The linear modes of vibration are used to discretize the system and the equations of motion are numerically integrated. Lepik [9] discusses elasto-plastic nonlinear vibrations of a buckled beam under harmonic excitation, with the aid of Galerkin's method. Vibrations that appear to be chaotic are found. In Ref. [10], a Shanley-type model is used to analyse elasto-plastic beam dynamics. A co-dimension three bifurcation problem is defined and the method of normal forms employed. Han and Lu [11] propose a space time FEM scheme for elasto-plastic dynamic analysis of Timoshenko beams. An isotropic hardening model is adopted and small displacements are considered. A cantilever beam under shock loading is analysed. In Ref. [12] a numerical algorithm for studying the development of plastic and damaged zones in a vibrating thin (Bernoulli–Euler) beam with guided rigid-body motion is presented. A linear elastic/perfectly plastic constitutive relation is adopted and small displacements assumed (geometrical nonlinearity is neglected, as often seems to occur). In Ref. [13] the previous analysis is extended and a linear elastic/perfectly plastic beam performing rotatory motions about a fixed hinged end is studied. A three-dof Shanley-type model is also used to investigate the dynamic instability of an elastic plastic beam in Ref. [14] and motions that apparently are chaotic are found. It is of particular interest to the present paper that the authors, in agreement with other authors, conclude that "A continuum beam model will be more appropriate to describe accurately the asymmetrical instability of the elastic–plastic beams".

Accurate models can be defined using the finite element method (FEM). However, the FE nonlinear equations of motion are solved by iterative methods and the computational effort can be substantial when the *h*-version of the FEM is employed, because this version, which is based on simple elements, often requires a large number of dof. In the so-called *p*-version FEM, the accuracy of the approximation is improved by increasing the number of shape functions over the elements. It has been widely shown that this version of the FEM demands a reduced number of dof to study vibrations linear or geometrically nonlinear (consult, for example, Refs. [3,4]). This version of the FEM has additional advantages, as not being prone to locking [4] and, if hierarchical,[1] possessing the embedding property [15]. The *p*-version of the FEM is applied in Ref. [16] to the deformation theory of plasticity, but only static problems are addressed. It is, once more, demonstrated that this is a very efficient strategy. However, apparently the *p*-version FEM has not been extended to elasto-plastic and geometrically nonlinear beam vibrations.

A procedure is proposed here to analyse the forced vibrations of beams oscillating in a plane, with large displacements and in the elasto-plastic regime. As explained in Section 2, the beam element is based on a first-order shear deformation theory, *p*-version finite element with hierarchical basis functions and the stresses are computed by the governing parameter method [6]. When a material is loaded in tension and then compressed, as occurs in cyclic loading, the yield stress in compression can be smaller than the yield stress reached in tension. A similar behaviour occurs when the material is again subjected to tension, and so on. This phenomenon is known as the Bauschinger effect [5,6] and none of the quoted references appears to have considered it. We will take into account Bauschinger effect by using a mixed hardening model. Section 3 is devoted to numerical tests; emphasis is given first to validation and analysis of convergence and, second, to the influence of plastic strains on the geometrically nonlinear beam vibrations. In Section 4, a summary of the conclusions is given.

2. Formulation

2.1. Relations between displacements, strains and stresses

A first-order shear deformation model will be followed, therefore, the displacement field is

$$u_1(x_1, x_3, t) = u_1^0(x_1, t) + x_3\theta^0(x_1, t) \tag{1}$$

[1]There are different notions of hierarchic FEM; here we follow Ref. [15] and consider an FEM as hierarchic if it is a *p*-version and uses a hierarchic set of shape functions.

$$u_3(x_1, x_3, t) = u_3^0(x_1, t) \tag{2}$$

where $u_i(x_1,x_3,t)$ is the displacement component along axis x_i and θ^0 (x_1,t) is the rotation of the cross section about axis x_2. The superscript 0 indicates the centroidal axis, x_1, which is also the longitudinal axis; x_3 is the vertical axis. The three reference axes are shown in Fig. 1.

Green strain (also known as Green–Lagrange strain) tensor [17] is

$$\varepsilon_{ij} = \frac{1}{2}\left(\frac{\partial u_i}{\partial x_j} + \frac{\partial u_j}{\partial x_i} + \frac{\partial u_k}{\partial x_i}\frac{\partial u_k}{\partial x_j}\right),$$

with $i, j, k = 1, 2, 3$. Displacements are here measured with respect to a stationary reference frame, connected to the undeformed or original configuration, an approach known as "total Lagrangian". Keeping only the nonlinear term $(\partial u_3/\partial x_1)^2$ in the longitudinal strain $\varepsilon_{11}(x_1,x_3,t)$, because the other nonlinear terms are most often negligible (Von Kármán approach), the longitudinal strain and the transverse shear engineering strain, $\gamma_{13}(x_1, t)$, are the following:

$$\varepsilon_{11}(x_1, x_3, t) = \frac{\partial u_1^0(x_1, t)}{\partial x_1} + \frac{1}{2}\left(\frac{\partial u_3^0(x_1, t)}{\partial x_1}\right)^2 + x_3\frac{\partial \theta^0(x_1, t)}{\partial x_1} \tag{3}$$

$$\gamma_{13}(x_1, t) = 2\varepsilon_{13}(x_1, t) = \frac{\partial u_3^0(x_1, t)}{\partial x_1} + \theta^0(x_1, t) \tag{4}$$

The longitudinal strain component can be written in a form that is advantageous to define the elemental stiffness matrices [4]:

$$\varepsilon_{11}(x_1, x_3, t) = \lfloor 1 \;\; x_3 \rfloor \left(\begin{Bmatrix} \varepsilon_0^p(x_1, t) \\ \varepsilon_0^b(x_1, t) \end{Bmatrix} + \begin{Bmatrix} \varepsilon_L^p(x_1, t) \\ 0 \end{Bmatrix} \right) \tag{5}$$

where the linear longitudinal strain, $\varepsilon_0^p(x_1, t)$, the bending strain, $\varepsilon_0^b(x_1, t)$, and the geometrically nonlinear longitudinal strain, ε_L^p, are defined as follows:

$$\varepsilon_0^p(x_1, t) = \frac{\partial u_1^0(x_1, t)}{\partial x_1}, \quad \varepsilon_0^b(x_1, t) = \frac{\partial \theta^0(x_1, t)}{\partial x_1}, \quad \varepsilon_L^p(x_1, t) = \frac{1}{2}\left(\frac{\partial u_3^0(x_1, t)}{\partial x_1}\right)^2 \tag{6}$$

The elastic constitutive relation is

$$\begin{Bmatrix} \sigma_{11}(x_1, x_3, t) \\ \sigma_{13}(x_1, x_3, t) \end{Bmatrix} = \begin{bmatrix} E & 0 \\ 0 & G \end{bmatrix} \begin{Bmatrix} \varepsilon_{11}(x_1, x_3, t) - \varepsilon_{11}^p(x_1, x_3, t) \\ \kappa\gamma_{13}(x_1, t) - \gamma_{13}^p(x_1, x_3, t) \end{Bmatrix} \tag{7}$$

where E is the Young modulus and G is the shear modulus of elasticity, which is equal to $E/(2(1+\nu))$. The letter ν represents the ratio of Poisson and κ is a shear correction factor. Only beams with rectangular cross section will be analysed, and we will most often assume that $\kappa = (5+5\nu)/(6+5\nu)$ (Ref. [18] defends this expression, apparently introduced by S.P. Timoshenko, for beams of rectangular cross section). $\varepsilon_{11}^p(x_1, x_3, t)$ represents the longitudinal plastic strain and $\gamma_{13}^p(x_1, x_3, t)$ the shear plastic strain. It is here assumed that stresses σ_{22}, σ_{33}, σ_{12} and σ_{23} are negligible.

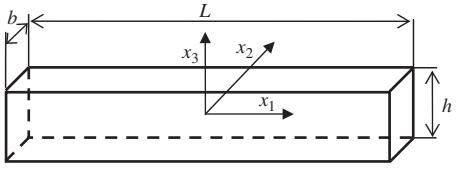

Fig. 1. Beam dimensions and reference axes.

2.2. Elemental matrices and equations of motion

In each element, the displacements on the centroidal axis are expressed in the form

$$\begin{Bmatrix} u_1^0(\xi,t) \\ u_3^0(\xi,t) \\ \theta^0(\xi,t) \end{Bmatrix} = \begin{bmatrix} \mathbf{N}^{u_1}(\xi)^{\mathrm{T}} & 0 & 0 \\ 0 & \mathbf{N}^{u_3}(\xi)^{\mathrm{T}} & 0 \\ 0 & 0 & \mathbf{N}^{\theta}(\xi)^{\mathrm{T}} \end{bmatrix} \begin{Bmatrix} \mathbf{q}_{u_1}(t) \\ \mathbf{q}_{u_3}(t) \\ \mathbf{q}_{\theta}(t) \end{Bmatrix} \tag{8}$$

$$\mathbf{N}^{u_1}(\xi)^{\mathrm{T}} = \{g_1(\xi), g_2(\xi), \ldots, g_{p_i}(\xi)\} \tag{9}$$

$$\mathbf{N}^{u_3}(\xi)^{\mathrm{T}} = \{f_1(\xi), f_2(\xi), \ldots, f_{p_0}(\xi)\} \tag{10}$$

$$\mathbf{N}^{\theta}(\xi)^{\mathrm{T}} = \{\Theta_1(\xi), \Theta_2(\xi), \ldots, \Theta_{p\theta}(\xi)\} \tag{11}$$

where the letter $\mathbf{q}$ is employed for time dependent generalized displacement vectors. The vectors of longitudinal, transverse and rotational shape functions are, respectively, $\mathbf{N}^{u_1}(\xi)$, $\mathbf{N}^{u_3}(\xi)$ and $\mathbf{N}^{\theta}(\xi)$. Functions $g_i(\xi)$, $f_i(\xi)$ and $\Theta_i(\xi)$ are the displacement shape functions, which belong to a set of polynomials of arbitrary high order [4]; to increase the accuracy of the model one increases the number of shape functions employed, keeping all the previously used functions (hence the designation *hierarchic*). In a 1D structure, the relation between the local coordinate, ξ, that appears in Eq. (8) and the global coordinate, x_1, is $x_1 = x_{1i} + \Delta x_{1i}/2 + \xi\,\Delta x_{1i}/2$, x_{1i} being the location of the left node of element number i and Δx_{1i} the element length. ξ varies from -1 to 1.

Applying the principle of virtual work, the following equation is obtained:

$$\int_{\Omega} \delta\varepsilon_{11}\sigma_{11}\,\mathrm{d}\Omega + \int_{\Omega} \delta\gamma_{13}\sigma_{13}\,\mathrm{d}\Omega - \int_{\Omega} \rho(\delta u_1\ddot{u}_1 + \delta u_3\ddot{u}_3)\,\mathrm{d}\Omega - \int_{\Omega} (\delta u_1 F_{u_1} + \delta u_3 F_{u_3} + \delta\theta M)\,\mathrm{d}\Omega = 0 \tag{12}$$

where F_{u_i} represents the forces with direction x_i and M represents the moment about x_2. The letter Ω denotes the integration domain, in this case the 3D region occupied by the beam. Employing relation (7), the first two terms of Eq. (12) are written as

$$\int_{\Omega} \delta\varepsilon_{11}\sigma_{11}\,\mathrm{d}\Omega = \int_{\Omega} \delta\varepsilon_{11}E\varepsilon_{11}\,\mathrm{d}\Omega - \int_{\Omega} \delta\varepsilon_{11}E\varepsilon_{11}^{p}\,\mathrm{d}\Omega \tag{13}$$

and

$$\int_{\Omega} \delta\gamma_{13}\sigma_{13}\,\mathrm{d}\Omega = \int_{\Omega} \delta\gamma_{13}\kappa G\gamma_{13}\,\mathrm{d}\Omega - \int_{\Omega} \delta\gamma_{13}G\gamma_{13}^{p}\,\mathrm{d}\Omega \tag{14}$$

In Eqs. (12)–(14) function arguments are not represented for the sake of simplicity.

At element level, the last term of Eq. (13) generates the following vectors:

$${}^{e}\mathbf{F}_{u_1}^{\mathrm{plast}}(\varepsilon_{11}^{p}) = E\frac{bh}{2}\int_{-1}^{1}\int_{-1}^{1} \mathbf{N}_{,\xi}^{u_1}(\xi)\varepsilon_{11}^{p}(\xi,\eta,t)\,\mathrm{d}\eta\,\mathrm{d}\xi \tag{15}$$

$${}^{e}\mathbf{F}_{\theta}^{\mathrm{plast}}(\varepsilon_{11}^{p}) = E\frac{bh^2}{4}\int_{-1}^{1}\int_{-1}^{1} \eta\mathbf{N}_{,\xi}^{\theta}(\xi)\varepsilon_{11}^{p}(\xi,\eta,t)\,\mathrm{d}\eta\,\mathrm{d}\xi \tag{16}$$

and matrix

$${}^{e}\mathbf{K}^{\mathrm{plast}}(\varepsilon_{11}^{p}) = E\frac{bh}{\Delta x_i}\int_{-1}^{1}\int_{-1}^{1} \mathbf{N}_{,\xi}^{w}(\xi)\mathbf{N}_{,\xi}^{w}(\xi)^{\mathrm{T}}\varepsilon_{11}^{p}(\xi,\eta,t)\,\mathrm{d}\eta\,\mathrm{d}\xi \tag{17}$$

${}^{e}\mathbf{F}_{u_1}^{\mathrm{plast}}$ and ${}^{e}\mathbf{F}_{\theta}^{\mathrm{plast}}$ are vectors of generalized forces that exist because of the longitudinal plastic strains; ${}^{e}\mathbf{K}^{\mathrm{plast}}$ is a matrix that appears due to the interaction between the plastic strains and the large displacements. The Young modulus, E, width, b, and thickness, h, are properties of the element and assumed to be constant within each element; the superscript e indicates that the vectors and matrix are elemental. The letter η represents the dimensionless coordinate in the x_3 direction.

The plastic shear strains also give rise to force vectors, which are defined as

$$ {}^{e}\mathbf{F}^{\text{plast}}_{\gamma u_3}(\gamma^p_{13}) = \frac{bh}{2} G \int_{-1}^{1}\int_{-1}^{1} \mathbf{N}^{w}_{,\xi}(\xi)\gamma^p_{13}(\xi,\eta,t)\,\mathrm{d}\eta\,\mathrm{d}\xi \tag{18} $$

$$ {}^{e}\mathbf{F}^{plast}_{\gamma\theta}(\gamma^p_{13}) = \frac{bh\,\Delta x_i}{4} G \int_{-1}^{1}\int_{-1}^{1} \mathbf{N}^{\theta}(\xi)\gamma^p_{13}(\xi,\eta,t)\,\mathrm{d}\eta\,\mathrm{d}\xi \tag{19} $$

By assembling the element force vectors and matrices, equations of motion of the following form are obtained:

$$ \begin{bmatrix} \mathbf{M}_{u_1} & \mathbf{0} & \mathbf{0} \\ \mathbf{0} & \mathbf{M}_{u_3} & \mathbf{0} \\ \mathbf{0} & \mathbf{0} & \mathbf{M}_{\theta} \end{bmatrix} \begin{Bmatrix} \ddot{\mathbf{q}}_{u_1}(t) \\ \ddot{\mathbf{q}}_{u_3}(t) \\ \ddot{\mathbf{q}}_{\theta}(t) \end{Bmatrix} + \begin{bmatrix} \mathbf{K}^{p}_{\ell_{11}} & \mathbf{0} & \mathbf{0} \\ \mathbf{0} & \mathbf{K}^{\gamma}_{\ell_{22}} & \mathbf{K}^{\gamma}_{\ell_{23}} \\ \mathbf{0} & \mathbf{K}^{\gamma}_{\ell_{32}} & \mathbf{K}^{\gamma}_{\ell_{33}} + \mathbf{K}^{b}_{\ell_{33}} \end{bmatrix} \begin{Bmatrix} \mathbf{q}_{u_1}(t) \\ \mathbf{q}_{u_3}(t) \\ \mathbf{q}_{\theta}(t) \end{Bmatrix} $$

$$ + \begin{bmatrix} \mathbf{0} & \mathbf{K}_{n\ell_{12}} & \mathbf{0} \\ \mathbf{K}_{n\ell_{21}} & \mathbf{K}_{n\ell_{22}} - K_{\text{plast}} & \mathbf{0} \\ \mathbf{0} & \mathbf{0} & \mathbf{0} \end{bmatrix} \begin{Bmatrix} \mathbf{q}_{u_1}(t) \\ \mathbf{q}_{u_3}(t) \\ \mathbf{q}_{\theta}(t) \end{Bmatrix} = \begin{Bmatrix} \mathbf{F}_{u_1}(t) \\ \mathbf{F}_{u_3}(t) \\ \mathbf{F}_{\theta}(t) \end{Bmatrix} + \begin{Bmatrix} \mathbf{F}^{\text{plast}}_{u_1}(\varepsilon^p_{11}) \\ \mathbf{F}^{\text{plast}}_{\gamma u_3}(\gamma^p_{13}) \\ \mathbf{F}^{\text{plast}}_{\theta}(\varepsilon^p_{11}) + \mathbf{F}^{\text{plast}}_{\gamma\theta}(\gamma^p_{13}) \end{Bmatrix} \tag{20} $$

Some of the matrices and vectors that appear in this equation are given in [4]. These are the mass matrices $\mathbf{M}_{u_1}$, $\mathbf{M}_{u_3}$ and $\mathbf{M}_{\theta}$; the so called linear stiffness matrices, written as $\mathbf{K}^{k}_{\ell_{ij}}$, where i, j are 1, 2 or 3, and k can be p, γ or b (standing for longitudinal, shear and bending, respectively); the geometrically nonlinear stiffness matrices $\mathbf{K}_{n\ell_{ij}}$, $i, j = 1,2$; and the vectors of generalized external forces $\mathbf{F}_{u_1}(t)$, $\mathbf{F}_{u_3}(t)$ and $\mathbf{F}_{\theta}(t)$. All these terms are computed resorting to analytical, exact, integration. The remaining forces and matrix $\mathbf{K}_{\text{plast}}$ were not included in [4]; they result from assembling the element vectors and matrix defined by Eqs. (15)–(19). Because they involve plastic strains, for which no analytical expression is known, these forces and matrix are computed using numerical integration [19] (in our case Gaussian integration).

2.3. Solution of the equations of motion and computation of plastic strains

The equations of motion are solved by the implicit Newmark scheme with Newmark's parameters [22]. The plastic terms are zero until yielding occurs. In a first cycle of the solution algorithm, the plastic strains from the previous time step—zero or not—are assumed to be invariant and used to compute the forces and matrix that are given by Eqs. (15)–(19). The generalized displacements are computed by solving Eq. (20) iteratively with update of the geometrically nonlinear stiffness matrix. Convergence in this cycle is achieved when the variation of the generalized displacements from one iteration to another is below a prescribed small value. Additionally, it is always verified whether the equation of motion (20) is satisfied.

After achieving convergence in the first cycle, the stresses are computed at the Gauss points using Eq. (7) and the Von Mises yield criterion with mixed hardening [6] is employed to verify if yielding occurred at any point. The yield function f_y is thus defined as

$$ f_y = \tfrac{1}{2}({}^{t+\Delta t}S_{ij}{}^{t+\Delta t}S_{ij} - {}^{t+\Delta t}\alpha_{ij}{}^{t+\Delta t}\alpha_{ij}) - \tfrac{1}{3}{}^{t+\Delta t}\sigma^2_y, \quad i,j = 1,2,3 \tag{21} $$

where α_{ij} are the components of the back stress tensor $\boldsymbol{\alpha}$, which are zero until plasticity takes place; ${}^{t+\Delta t}\sigma_y$ is the yield stress, which is plasticity dependent, and S_{ij} are the deviatoric stress components given by

$$ S_{ij} = \sigma_{ij} - \sigma_m \delta_{ij} \tag{22} $$

with σ_m the mean stress and δ_{ij} the Kronecker delta. In the case of beams: $S_{11} = 2\sigma_{11}/3$, $S_{22} = S_{33} = -\sigma_{11}/3$, $S_{13} = S_{31} = \sigma_{13}/3$, $S_{12} = S_{21} = S_{23} = S_{32} = 0$.

The summation convention applies in Eq. (21), where the nine deviatoric stress components—a second-order tensor—are written in vector form, i.e., $\mathbf{S} = \{S_{11}, S_{12}, S_{13}, S_{21}, \ldots, S_{33}\}$. This vector form is also used in this text for the other second-order tensors related with stress and strain.

If yielding occurs at a Gauss point, the plastic strains and the plastic dependent variables, including the yield stress, must be updated. It is also necessary to re-compute the generalized displacements from (20). These tasks are carried out in a second cycle. To compute the plastic strains, the governing parameter method with the increment of effective plastic strain, Δe^P, as governing parameter is employed. The procedure is briefly described here and Ref. [6] may be consulted for further elucidation.

To apply the governing parameter method, the Von Mises yield function was chosen as a governing function. If, as assumed here, the stress–strain relation is bilinear, Fig. 2, the yield function can be written as

$$f_y(\Delta e^P) = \frac{{}^{t+\Delta t}\sigma^E}{{}^{t+\Delta t}\sigma_y + [3G + (1-M)E_P]\Delta e^P} - 1 \tag{23}$$

The first step in the governing parameter method is to compute Δe^P by equating the governing function $f_y(\Delta e^P)$ to zero.

The constant M in Eq. (23) is the mixed hardening parameter, a characteristic of the material that represents a measure of the Bauschinger effect. In a mixed hardening material model, which is between isotropic and kinematic hardening material models, only the isotropic part $M(e^P + \Delta e^P)$ of the effective plastic stress affects the size of the yield surface [6]. The back stress, $\boldsymbol{\alpha}$, introduced in Eq. (21) defines the position of the yield surface. This position changes when the Bauschinger effect occurs.

The plastic modulus E_p that appears in Eq. (23) can be expressed in terms of the tangent, E_T, and Young, E, modulus as

$$E_P = \frac{EE_T}{E - E_T} \tag{24}$$

In a bilinear stress–strain relation E_T and E_P are constants.

${}^{t+\Delta t}\sigma^E$, in Eq. (23), is the value of the effective plastic stress when $\Delta e^P = 0$, which is given by

$${}^{t+\Delta t}\sigma^E = \left(\tfrac{3}{2}{}^{t+\Delta t}\hat{\mathbf{S}}^E \cdot {}^{t+\Delta t}\hat{\mathbf{S}}^E\right)^{1/2} \tag{25}$$

${}^{t+\Delta t}\hat{\mathbf{S}}^E$ is the radius of elastic stress surface, defined as

$${}^{t+\Delta t}\hat{\mathbf{S}}^E = {}^{t+\Delta t}\mathbf{S}^E - {}^{t}\boldsymbol{\alpha} \tag{26}$$

${}^{t+\Delta t}\mathbf{S}^E$ is the deviatoric stress of the elastic solution, i.e., the solution with no plastic deformation in the current step. This may be computed using the following equations:

$${}^{t+\Delta t}e'_{ij} = {}^{t+\Delta t}\varepsilon_{ij} - {}^{t+\Delta t}\varepsilon_m, \quad i = j \tag{27}$$

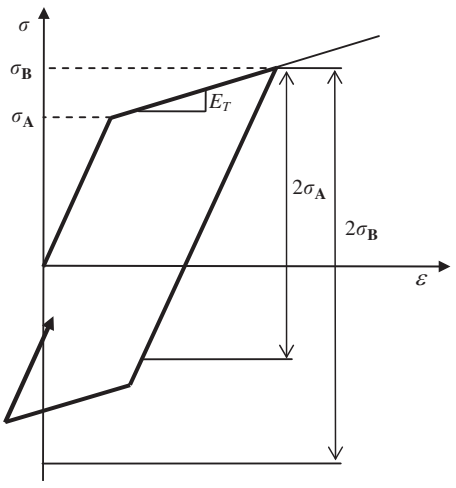

Fig. 2. Bilinear uniaxial stress–strain curve with mixed hardening. The yield stress in compression is smaller than $\sigma_{\mathbf{B}} - 2\sigma_{\mathbf{A}}$ and larger than $-\sigma_{\mathbf{B}}$.

$$^{t+\Delta t}e'_{13} = \tfrac{1}{2}{}^{t+\Delta t}\gamma_{13} \tag{28}$$

$$^{t+\Delta t}e''_{ij} = {}^{t+\Delta t}e'_{ij} - {}^{t}\varepsilon^{P}_{ij} \tag{29}$$

$$^{t+\Delta t}\mathbf{S}^{E} = 2G^{t+\Delta t}\mathbf{e}'' \tag{30}$$

with $^{t+\Delta t}e'_{ij}$ the components of the deviatoric strain tensor and $^{t}\varepsilon^{P}_{ij}$ the components of the plastic strain tensor in the previous step.

In the case of beams $\sigma_{22} = \sigma_{33} = 0$ and, therefore,

$$^{t+\Delta t}\varepsilon_{11} = {}^{t+\Delta t}\frac{\sigma_{11}}{E} + {}^{t+\Delta t}\varepsilon^{P}_{11}, \quad {}^{t+\Delta t}\varepsilon_{22} = -\frac{v}{E}{}^{t+\Delta t}\sigma_{11} + {}^{t+\Delta t}\varepsilon^{P}_{22}, \quad {}^{t+\Delta t}\varepsilon_{33} = -\frac{v}{E}{}^{t+\Delta t}\sigma_{11} + {}^{t+\Delta t}\varepsilon^{P}_{33} \tag{31}$$

Moreover, because the volumetric plastic strain equals zero ($\varepsilon^{P}_{V} = {}^{t+\Delta t}\varepsilon^{P}_{11} + {}^{t+\Delta t}\varepsilon^{P}_{22} + {}^{t+\Delta t}\varepsilon^{P}_{33} = 0$), the mean strain—required in Eq. (27)—is given by

$$^{t+\Delta t}\varepsilon_{m} = \frac{1-2v}{3}\frac{\sigma_{11}}{E} \tag{32}$$

Parameter $\Delta\lambda$, a positive factor of proportionality that relates the increments of plastic strain and the total deviatoric stresses, is given by

$$\Delta\lambda = \frac{3}{2}\frac{\Delta e^{P}}{^{t+\Delta t}\sigma_{y}} \tag{33}$$

where the yield stress is given by

$$^{t+\Delta t}\sigma_{y} = \sigma_{yv} + ME_{P}(e^{P} + \Delta e^{P}) \tag{34}$$

σ_{yv} is the initial yield stress, i.e., the yield stress before any plastic hardening occurred.

The stress radius $^{t+\Delta t}\hat{\mathbf{S}}$, which is the deviatoric stress minus the back stress, can be computed from

$$^{t+\Delta t}\hat{\mathbf{S}} = \frac{^{t+\Delta t}\hat{\mathbf{S}}^{E}}{1 + 2[G + (1-M)E_{P}/3]\Delta\lambda} \tag{35}$$

an equation that is only valid in a bilinear stress–strain relation. To arrive at Eq. (35) one uses the fact that the deviatoric stresses (22) can also be given by

$$^{t+\Delta t}\mathbf{S} = {}^{t+\Delta t}\mathbf{S}^{E} - 2G\Delta\lambda^{t+\Delta t}\hat{\mathbf{S}} \tag{36}$$

The increment of plastic strains is given by the Prandtl–Reuss equations:

$$\Delta^{t+\Delta t}\boldsymbol{\varepsilon}^{P} = \Delta\lambda^{t+\Delta t}\hat{\mathbf{S}} \tag{37}$$

but where $^{t+\Delta t}\hat{\mathbf{S}}$ are the deviatoric stresses $^{t+\Delta t}\mathbf{S}$, defined in Eq. (22), minus the back stresses $^{t+\Delta t}\boldsymbol{\alpha}$. The total plastic strain at time $t+\Delta t$ is

$$^{t+\Delta t}\boldsymbol{\varepsilon}^{P} = {}^{\Delta t}\boldsymbol{\varepsilon}^{P} + \Delta\boldsymbol{\varepsilon}^{P} \tag{38}$$

and the back stress is given by

$$^{t+\Delta t}\boldsymbol{\alpha} = {}^{\Delta t}\boldsymbol{\alpha} + \Delta\boldsymbol{\alpha} \tag{39}$$

$$\Delta\boldsymbol{\alpha} = 2(1-M)E_{P}\Delta\boldsymbol{\varepsilon}^{P}/3 \tag{40}$$

Eq. (40) is a form of Prager's hardening rule [6] where $2E_P/3$ is the kinematic hardening modulus.

Now that the plastic strains have been computed, the forces and matrix given by Eqs. (15)–(19) can be updated. It is then required to return to the equations of motion (20) and correct the generalized displacements in an inner iterative procedure where the geometrically nonlinear terms are corrected. When convergence is achieved in this inner iterative procedure, the new generalized displacements are used to compute the strains and stresses. Then one verifies if convergence has also been achieved in the computation of the plastic strains and back stresses. In the positive case, one proceeds to the next time step, otherwise one returns to the

computation of the plastic strains using Eqs. (21)–(40) and the updated generalized displacements. Hence, the iterations in a particular time step only stop when neither the generalized displacements, nor the plastic strains vary more than accepted threshold values. The solution is always enforced to be inside or on the yield surface.

3. Numerical tests

3.1. Validation and analysis of convergence

To somehow validate the approach here suggested and the computational code implemented, a few examples were carried out. The first example is taken from Ref. [8], where vibrations of an elasto-plastic beam of steel with properties $v = 0.3$, $E = 2.06 \times 10^{11}\,\mathrm{N\,m^{-2}}$, $\rho = 7.69 \times 10^{3}\,\mathrm{kg\,m^{-3}}$, $\sigma_{yv} = 4.88 \times 10^{8}\,\mathrm{N\,m^{-2}}$, were analysed. The tangent modulus E_T is not given in Ref. [8], where a different hardening parameter is employed, and we used $E_T = 10^{9}\,\mathrm{N\,m^{-2}}$ from an example in Ref. [6]. Parameter M was assumed to be 1 (isotropic hardening). The geometric properties of this beam are $b = 0.02\,\mathrm{m}$, $L = 0.406\,\mathrm{m}$ and $h = 0.2L$. The excitation is provided by a distributed, transverse, step force with amplitude $0.00429\ EA/L\,\mathrm{N\,m^{-1}}$ and with duration $2.3c/L\,\mathrm{s}$, where c represents the speed of sound in steel, given by $c = \sqrt{E/\rho}$. The beam is clamped at both ends (CC) and undamped.

Fig. 3 shows the longitudinal plastic strain at three instants, which can be compared with the distribution of plastic zones shown in Fig. 7 of Ref. [8]. Both analyses show that initially the plastic zones appear close to the clamped ends and later develop to the centre of the beam; in spite of the differences in the formulation and approximation methods the agreement is quite good.

The following tests involve comparison with results obtained using the FEM code ANSYS. Before proceeding to the inelastic analysis, a convergence study in the computation of the linear natural frequencies is carried out. The beam material and geometric properties are now the following: $v = 0.3$, $E = 2.00 \times 10^{11}\,\mathrm{N\,m^{-2}}$, $\rho = 7.8 \times 10^{3}\,\mathrm{kg\,m^{-3}}$, $b = 0.03\,\mathrm{m}$, $L = 1\,\mathrm{m}$ and $h = 0.01L$. These properties were taken from an example shown in Ref. [21], and will accompany us in the next numerical tests. The two ANSYS elements employed are BEAM23, with shear deflection, and SHELL43. The BEAM23 element has two nodes and three dof at each node: two displacements and one rotation. The SHELL43 element has four nodes, with six dof at each node: translations in the nodal x_1, x_2 and x_3 directions and rotations about the nodal x_1, x_2 and x_3 axes. Both elements have plasticity and large deflection capabilities, which will be required in an ensuing example. The ANSYS beam element follows a first-order shear deformation approach similar to the one employed in our formulation and the shell element is here employed to obtain reference results, since shell theory resorts to less approximations than beam theory.

The first six linear natural frequencies of modes of vibration in the plane x_1x_3 are shown in Table 1 (ANSYS, h-version FEM, results) and in Table 2 (p-version FEM results). Values computed with different meshes in ANSYS are shown in order to give an idea of the convergence rate of the h-version elements. Two shear correction factors are employed in the p-version element; the first is the more traditional $\frac{5}{6}$, which is also employed in the ANSYS code, and the second is $\kappa = (5+5v)/(6+5v)$, which was mentioned in Section 2. The same numbers of transverse, longitudinal and rotational shape functions are employed in each p-element.

By comparing the natural frequencies computed with the beam element of ANSYS with the ones computed with the p-version and the same shear correction factor ($\kappa = \frac{5}{6}$), one confirms that the two models give very similar values and that the p-version requires fewer dof for equivalent accuracy levels. In fact, the 51 dof

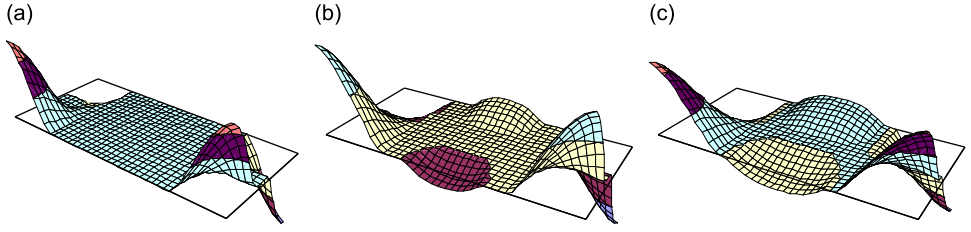

Fig. 3. Longitudinal plastic strain along CC beam subjected to rectangular pulse: (a) $t = 0.94\ L/c$, (b) $t = 1.33\ L/c$, (c) $t = 2.1\ L/c$.

Table 1
Linear natural frequencies of vibration (Hz) computed with ANSYS elements.

Element type	BEAM23	BEAM23	BEAM23	BEAM23	SHELL43	SHELL43	SHELL43
Number of elements	20	40	80	100	400	1600	6400
dof	63	117	237	297	3582	11970	43146
Mode number							
1	52.015	52.015	52.015	52.015	52.043	52.035	52.031
2	143.25	143.25	143.25	143.25	143.34	143.31	143.30
3	280.51	280.49	280.48	280.48	280.70	280.62	280.59
4	463.06	462.95	462.93	462.93	463.37	463.19	463.12
5	690.65	690.29	690.24	690.24	691.01	690.69	690.56
6	963.04	962.07	961.94	961.93	963.20	962.66	962.44

Table 2
Linear natural frequencies of vibration (Hz) computed with *p*-version elements.

Dof	51[a]	69[a]	75[a]	39[b]	51[b]	69[b]	75[b]
Mode number							
1	52.015	52.015	52.015	52.016	52.016	52.016	52.016
2	143.25	143.25	143.25	143.26	143.26	143.26	143.26
3	280.49	280.49	280.49	280.52	280.52	280.51	280.51
4	462.95	462.94	462.94	463.03	463.02	463.01	463.01
5	690.28	690.26	690.26	690.45	690.42	690.40	690.40
6	962.02	961.98	961.97	962.39	962.27	962.23	962.22

[a]Shear correction factor $\frac{5}{6}$.
[b]Shear correction factor $(5+5\nu)/(6+5\nu)$.

p-version element provides frequencies that are either equal or closer to the ones of more refined models (the 75 dof *p*-version and 297 dof ANSYS *h*-version) than the 117 dof ANSYS *h*-version element model. It should be noted that, although it would be very straightforward, we did not resort to any type of reduction of the *p*-version model size. Had we, for example, not included the longitudinal generalized coordinates in the *p*-version model, the results would have been exactly the same, with $\frac{2}{3}$ of the dof.

As far as the shear correction factor is concerned, the frequencies computed with $\kappa=(5+5\nu)/(6+5\nu)$, Table 2, are closer than the ones computed using $\kappa=\frac{5}{6}$ to the frequencies computed with the ANSYS shell element in Table 1. The choice of $\kappa=(5+5\nu)/(6+5\nu)$ as shear correction factor hence appears to be appropriate.

In a test involving plasticity, static analyses are carried out in ANSYS and the results are compared with the *p*-version ones. The beam is the one analysed in the previous example; the yield stress, $\sigma_{yv}=2.0\times10^8\,\mathrm{N\,m^{-2}}$, is taken from an example of Ref. [6] and the tangent modulus is $E_T=10^8\,\mathrm{N\,m^{-2}}$, which is somewhat small, approaching the popular elastic–perfectly plastic model [6]. M is again 1. A constant point force with variable amplitude is applied in the middle of the beam, upwards (positive) in the vertical direction. In the *p*-version models a transient problem was actually solved, using the code based on the Newmark method that will be also employed in vibration analysis: a step force was applied and a large damping considered in order to avoid overshoot; in these conditions the limit value of the displacement is equivalent to the static one. Two *h*-version finite element models (ANSYS) are considered; one employs 40 planar beam elements BEAM23, with shear deflection, and the other is an extremely detailed shell model that will be used as reference. The latter model employs 6400 SHELL43 elements (eight elements in the thickness direction by 800 in the length).

Results computed with several *p*-version elements are presented in Table 3; all employ 40 Gauss points in the longitudinal direction and 20 in the transverse direction. The relative error with respect to the shell model values is given between brackets. The *p*-version models give displacement amplitudes that are reasonably close to the very detailed ANSYS shell model, which has 43 146 dof. With a curious exception at 2000 N, the *p*-version element provides more accurate results and requires far fewer dof than the *h*-version beam element

Table 3
Non-dimensional (u_3/h) displacements in the middle of a beam under a constant transverse force.

Force (N)	p-version, 39 dof	p-version, 51 dof	p-version, 69 dof	p-version, 69 dof, $\kappa=\frac{5}{6}$	p-version, 75 dof	BEAM23 ANSYS, 117 dof	SHELL43 ANSYS, 43 146 dof	Regime
500	0.45371 (−0.086%)	0.45401 (−0.019%)	0.45416 (0.014%)	0.45418 (0.018%)	0.45419 (0.020%)	0.45470 (0.13%)	0.45410	Elastic
1000	0.74581 (−0.17%)	0.74647 (−0.078%)	0.74677 (−0.038%)	0.74679 (−0.034%)	0.74682 (−0.031%)	0.74948 (0.33%)	0.74705	Elasto-plastic
1500	0.97573 (−0.99%)	0.97943 (−0.62%)	0.98213 (−0.34%)	0.98215 (−0.34%)	0.98280 (−0.28%)	0.98000 (−0.56%)	0.98551	Elasto-plastic
2000	1.2149 (−3.0%)	1.2264 (−2.1%)	1.2379 (−1.2)	1.2379 (−1.2%)	1.2391 (−1.1%)	1.2528 (0.024%)	1.2525	Elasto-plastic
2500	1.4530 (−5.4%)	1.4758 (−3.9%)	1.4950 (−2.6%)	1.4951 (−2.6%)	1.4989 (−2.4%)	1.4896 (−3.0%)	1.5352	Elasto-plastic

p-version results with 40×20 Gauss points. $\kappa=(5+5\nu)/(6+5\nu)$ except where indicated $\kappa=\frac{5}{6}$.

Table 4
Non-dimensional (u_3/h) displacements in the middle of a beam under a constant transverse force.

Force (N)	p-version, 69 dof					p-version, 75 dof	SHELL43 ANSYS, 43 146 dof	Regime
	20×10 GP	32×32 GP	40×20 GP	64×32 GP	64×64 GP	64×64 GP		
500	0.45416 (0.014%)	0.45416 (0.014%)	0.45416 (0.014%)	0.45416 (0.014%)	0.45416 (0.014%)	0.45419 (0.020%)	0.45410	Elastic
1000	0.74678 (−0.036%)	0.74677 (−0.037%)	0.74677 (−0.037%)	0.74678 (−0.036%)	0.74678 (−0.036%)	0.74684 (−0.028%)	0.74705	Elasto-plastic
1500	0.98016 (−0.54%)	0.98250 (−0.31%)	0.98213 (−0.34%)	0.98234 (−0.321%)	0.98242 (−0.31%)	0.98297 (−0.26%)	0.98551	Elasto-plastic
2000	1.2386 (−1.1%)	1.2371 (−1.2%)	1.2379 (−1.2%)	1.2385 (−1.1%)	1.2386 (−1.1%)	1.2399 (−1.0%)	1.2525	Elasto-plastic
2500	1.5184 (−1.1%)	1.4948 (−2.6%)	1.4950 (−2.6%)	1.4990 (−2.4%)	1.4997 (−2.3%)	1.5039 (−2.0%)	1.5352	Elasto-plastic

Convergence with the number of Gauss points (GP). p-version 69 dof (3×23) model with shear correction factor $\kappa=(5+5\nu)/(6+5\nu)$.

of ANSYS. Moreover, the plastic zones obtained with the p-version beam finite element were visually compared with the ones resulting from the very detailed shell model and the agreement is quite reasonable; the h-version beam element of ANSYS does not provide as detailed a distribution of the plastic zones.

On the down side—a disadvantage that should be common to any approximation method—it is noticeable that the number of dof required for convergence increases as the nonlinear terms due to geometrical nonlinearity and plasticity increase (i.e., as the applied force amplitude increases). More dof are required in this geometrical nonlinear and elasto-platic problem than in the computation of the linear natural frequencies, which is a linear elastic problem.

Concerning the two shear correction factors—$(5+5\nu)/(6+5\nu)$ and $5/6$; see results from p-version model with 69 dof—the displacements computed with $\kappa=(5+5\nu)/(6+5\nu)$ are closer to the ones computed with the ANSYS shell element when the force amplitude is not large. At some of the larger forces the shear correction factor $\frac{5}{6}$ provided displacements marginally closer—distinction in the fifth significant digit only—to the ones of the ANSYS shell model. Hence, in the simultaneously inelastic and geometrical nonlinear tests $\kappa=(5+5\nu)/(6+5\nu)$ performed either similarly or very marginally worse than factor $\kappa=5/6$. Given the superiority of the shear correction factor $\kappa=(5+5\nu)/(6+5\nu)$ in the computation of the natural frequencies, we will adopt $\kappa=(5+5\nu)/(6+5\nu)$ in the dynamic analyses.

Table 4 presents non-dimensional displacement mostly computed with the 69 dof p-version beam finite element and using different numbers of Gauss points. When 20×10 Gauss points are employed in the 69 dof p-element, the displacements in the middle of the beam are already very close to the ones computed with the very detailed 43 146 dof shell model. Actually, in a few of the tests results closer to the shell ones are computed

with 20×10 Gauss points than with more integration points. A possible explanation for this fact is that by using a smaller number of Gauss integration points the stiffness is artificially reduced, thus increasing the displacement amplitude and approaching the more flexible shell model. In any case, using 64×64 Gauss points similar or better results are, with one exception, obtained. Moreover, a visual comparison of surfaces defined by the plastic strains and total stresses revealed, as expected, that the larger the number of Gauss points employed in the p-model, the more detailed and smoother the computed surfaces become (examples are given in the next section).

Data computed with a 75 dof p-element and 64×64 Gauss points is also given in Table 4; this element provides amplitudes that differ between -0.020 and 2.0 percent amplitudes computed with the 43 146 dof shell model.

Another test was carried out to verify how the program behaves with a different tangent modulus; the geometric and material properties are similar to the previous ones, with the exception of E_T, which is now $10^9\,\mathrm{N\,m^{-2}}$, a value for steel taken from Ref. [6]. An analysis of convergence was carried out. Table 5 gives a summary of the data, all in the elasto-plastic regime. In comparison with the previous example, the displacements are lower, because with a larger tangent modulus the internal forces increase more with the strains. Taking the 43 146 dof shell model as reference, the error of the beam p-version models is always below 1.86 percent. As occurred in the case with $E_T = 10^8\,\mathrm{N\,m^{-2}}$, the implemented numerical procedure was able to solve the equations of motion.

The following test example is taken from Ref. [21]. Most of the beam material and geometric properties, including the yield stress—which is not given in Ref. [21] because plasticity is not addressed there—are the ones of the former example. Mass proportional viscous damping with a proportionality factor β equal to one is assumed. This means that the equations of motion (20) take the form

$$\mathbf{M}\ddot{\mathbf{q}} + \beta\mathbf{M}\dot{\mathbf{q}} + \mathbf{K}_{\ell}\mathbf{q} + [\mathbf{K}_{n\ell} - \mathbf{K}_{\mathrm{plast}}]\mathbf{q} = \mathbf{F} + \mathbf{F}^{\mathrm{plast}} \tag{41}$$

The excitation is transverse, uniformly distributed along the clamped–clamped beam. Two tangent moduli were considered, $E_T = 10^8\,\mathrm{N\,m^{-2}}$ and $E_T = 10^9\,\mathrm{N\,m^{-2}}$, to see if numerical problems occur due to parameter values. As said before, the former modulus turns the model closer to the one of perfectly plastic materials and the latter is taken from an example of Ref. [6]. However, in this section only results with $E_T = 10^8\,\mathrm{N\,m^{-2}}$ are shown; values computed with $E_T = 10^9\,\mathrm{N\,m^{-2}}$ are shown in the next section. M is again 1.

Fig. 4 shows the steady state displacement time history at the middle point of the beam when the excitation frequency is 117.8097 rad/s ($\cong$18.75 Hz) and the excitation amplitude $1000\,\mathrm{N\,m^{-1}}$. The displacement time history resembles that of Fig. 7(a) of Ref. [21] but small plastic strains were found near the clamped ends. The longitudinal plastic strains in steady state and at four points are shown in Fig. 5. The coordinates of the points are: Point 1 $(\xi,\eta) = (0.9907,-0.8391)$, Point 2 $(\xi,\eta) = (0.9982,-0.8391)$, Point 3 $(\xi,\eta) = (0.9579,0.8391)$, Point 4 $(\xi,\eta) = (0.9982,0.9931)$. These points are near the beam limits where the plastic strains experience steep variations; therefore, an accurate computation of the plastic strains requires employing high-order shape functions. It is clear that the values of plastic strains change more with the number of shape functions employed in the element than the linear natural frequencies (Table 1). In this example, the plastic strains are of small consequence in the transverse displacement, as is shown in Fig. 4, which relates to the middle point of the beam. This was also found to be the case in points near the clamped ends (figure not included).

Table 5
Non-dimensional (u_3/h) displacements in the middle of a beam under a constant transverse force, $E_T = 10^9\,\mathrm{N\,m^{-2}}$, shear correction factor $\kappa = (5+5\nu)/(6+5\nu)$.

Force (N)	69 dof p-version, 40×20 GP	69 dof p-version, 64×64 GP	75 dof p-version, 40×20 GP	75 dof p-version, 64×64 GP	SHELL43 ANSYS, 43 146 dof
1500	0.98250 (−0.26%)	0.98267 (−0.25%)	0.98254 (−0.26%)	0.98271 (−0.24%)	0.98511
2000	1.2360 (−0.94%)	1.2367 (−0.89%)	1.2361 (−0.94%)	1.2367 (−0.89%)	1.2478
2500	1.4879 (−1.85%)	1.4916 (−1.6%)	1.4880 (−1.8%)	1.4917 (−1.6%)	1.5160

Relative errors between brackets, using the shell model as reference.

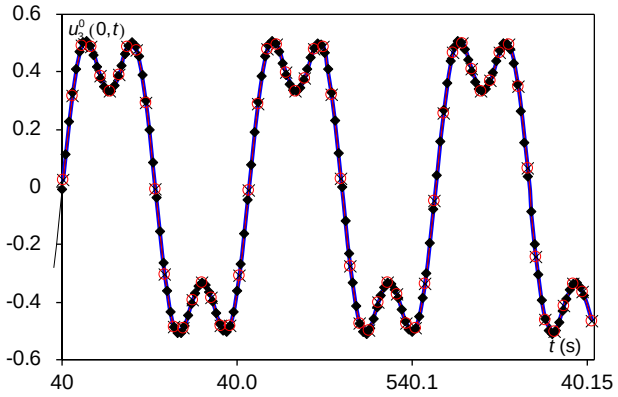

Fig. 4. Transverse displacement at middle point of the beam, computed with 40×20 Gauss points and: -21 dof, -○- 33 dof, - × - 69 dof, computed wit 64×64 Gauss points and ♦ 75 dof.

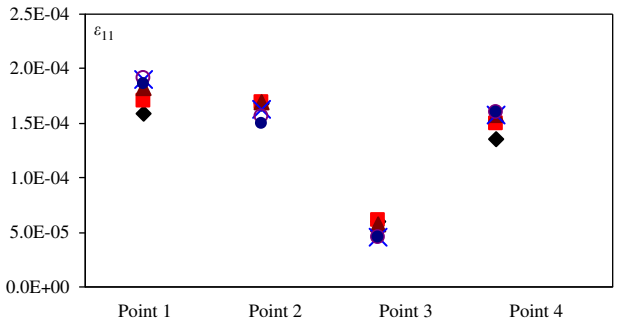

Fig. 5. Longitudinal plastic strains computed with 40×20 Gauss points and: ♦ 21 dof, ■ 27 dof, ▲ 33 dof, × 51 dof; ○ 69 dof, ● 75 dof.

3.2. Numerical analysis of the influence of plastic terms on forced vibrations

In the former section convergence studies were carried out. Different parameters were considered in order to see if the procedure implemented experiences any convergence difficulties and if it approaches values that were either published or obtained with a well known FE code. The goal of the present section is to show the effect of the plastic strains on the forced vibrations of beams vibrating in the geometrically nonlinear regime. The *p*-version model employed in this section has a total of 75 dof and 64×64 Gauss points. In the former section it was verified that this model is superior to models based on *h*-version beam finite elements and that it approaches very reasonably a shell model based on *h*-version finite elements, which employs far more dof. The geometric and the linear elastic material properties—typical of steel—are taken from Ref. [21], and are the ones used in the last examples of the former section. The tangent modulus of all examples of the present section is $E_T = 10^9\,\mathrm{N\,m^{-2}}$ and the yield stress before yielding occurs is $\sigma_{yv} = 2.0 \times 10^8\,\mathrm{N\,m^{-2}}$, values that are also appropriate for some steels and taken from Ref. [6]. The first test with this data was a replica of the last test of the former section, where E_T was $10^8\,\mathrm{N\,m^{-2}}$. Data from the test with $E_T = 10^9\,\mathrm{N\,m^{-2}}$ is not shown here, since the values of the transverse displacements were virtually the same, because the plastic strains are small in this example (zero in most of the beam). Naturally, the plastic strains computed with $E_T = 10^9\,\mathrm{N\,m^{-2}}$ differ from the ones computed with $E_T = 10^8\,\mathrm{N\,m^{-2}}$, but only slightly.

Fig. 6 shows the transverse displacement time history of a point located at the middle of the beam, when the excitation frequency is equal to the first linear natural frequency, 326.827 rad/s, and the amplitude of the distributed transverse force is $500\,\mathrm{N\,m^{-1}}$. Also shown is the projection of the trajectory on the phase plane defined by the transverse displacement and velocity. T_e represents the excitation period. Compared with the geometrically nonlinear and purely elastic results, the motion with plastic strains achieves smaller

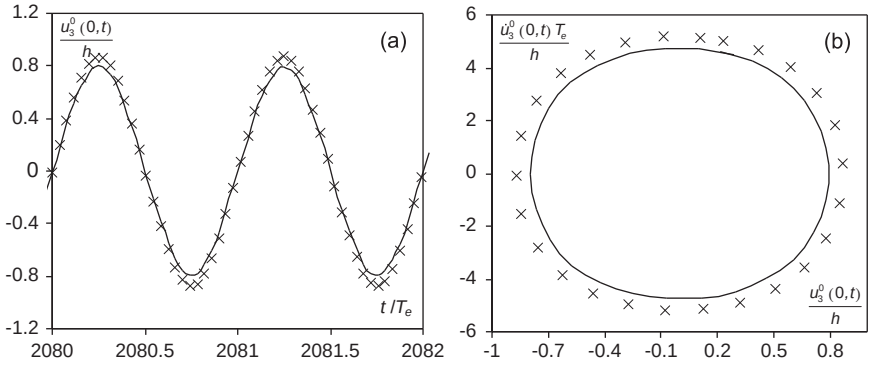

Fig. 6. (a) Transverse displacement of middle point and (b) projection on a phase plane, excitation at first linear natural frequency with $500\,\mathrm{N\,m^{-1}}$ amplitude: — elasto-plastic and geometrically nonlinear; × geometrically nonlinear.

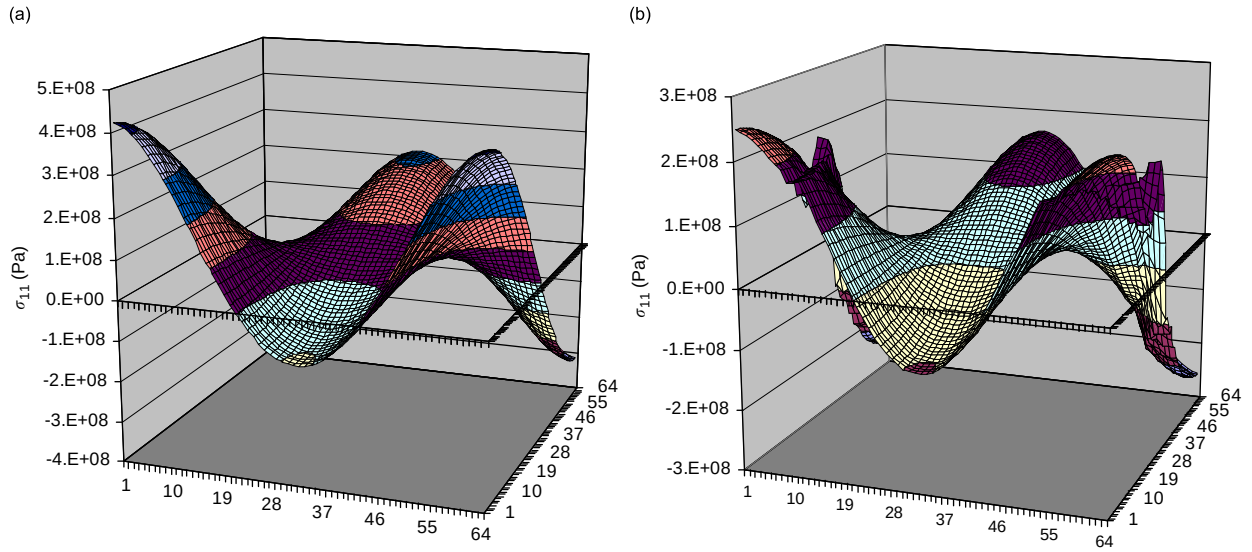

Fig. 7. Stresses σ_{11} computed with linear elastic model (a) and with elasto-plastic model (b), when $t = 0.75548\,\mathrm{s}$, excitation at linear natural frequency with $500\,\mathrm{N\,m^{-1}}$ amplitude.

displacement and velocity amplitudes. In spite of the presence of the plastic strains, the oscillation remains periodic and dominated by the excitation frequency.

Fig. 7 shows the longitudinal stresses, σ_{11}, computed with the linear elastic model and with the elasto-plastic model, both geometrically nonlinear, at a particular instant ($t = 0.75548\,\mathrm{s}$). The values obtained differ more near the clamps and in the middle of the beam due to the plastic strains. The surface defined by σ_{11} becomes somewhat irregular near the clamps when plasticity is taken into account. This effect, which was not at all so profound in the static cases of the former section, appears to be a consequence of the cyclic load. The stresses computed without considering plastic strains attain values over 400 MPa; therefore, plasticity would occur even if the steel was a higher strength one.

In the following test, a beam with similar characteristics but thicker ($h = 0.05L$) is analysed. The force amplitude was increased to $10\,000\,\mathrm{N\,m^{-1}}$ in order to achieve large displacements. The damping factor β (see Eq. (41)) was chosen so that the non-dimensional damping ratio, which is equal to the viscous damping coefficient divided by the critical damping coefficient [23], of a single dof system representing the beam does not change. Therefore, β is now 4.92206.

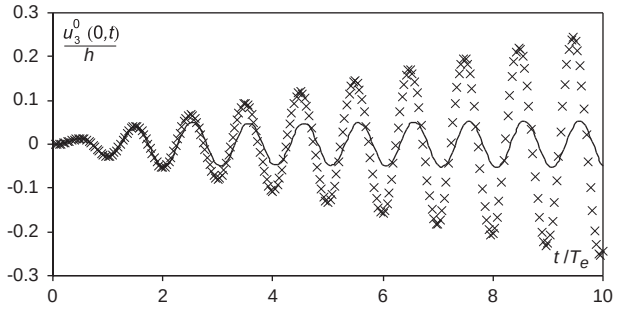

Fig. 8. First cycles of transverse displacement of middle point of thick beam, excitation at linear natural frequency with 10 000 N m^{-1} amplitude: — elasto-plastic and geometrically nonlinear; × geometrically nonlinear, linear elastic.

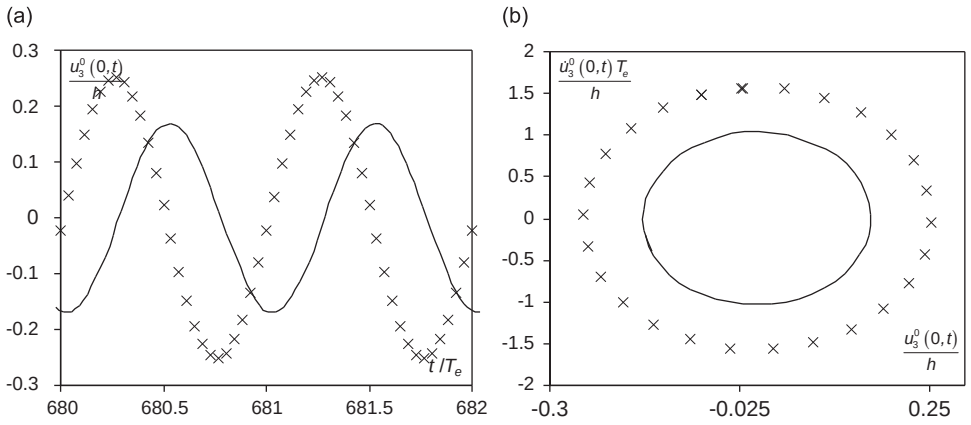

Fig. 9. (a) Transverse displacement of middle point and (b) projection on a phase plane; later cycles of transverse displacement of middle point of thick beam, excitation at linear natural frequency with 10 000 N m^{-1} amplitude: — elasto-plastic and geometrically nonlinear; × geometrically nonlinear, linear elastic.

Fig. 8 shows the evolution of the transverse displacement during the first 10 excitation cycles. The model that only includes geometrically nonlinear terms (i.e., neglects the plastic strains) grossly over-predicts the displacement amplitude, because it neglects the energy that is dissipated as plastic strains are developed. Fig. 9 shows the transverse displacement and the projection of the trajectory on a phase plane at later cycles. The geometrically nonlinear, linear elastic model still over predicts the displacement and velocity amplitudes, possibly because the plastic strains change the natural frequency of the beam to one that is further away from this particular excitation frequency. At this stage the plastic strains are not changing in almost all the beam (there are still small changes in some points), hence there is only a small dissipation due to plastic work. The plastic strains at instant 2.66736 s ($t/T_e = 682.913$) are shown in Fig. 10, revealing that they mainly develop close to the clamped boundaries.

Numerical tests also show that the displacements obtained by the elastic–plastic geometrical nonlinear model can be larger than the ones obtained by using only the elastic model, due to softening induced by plasticity. An example is shown in Fig. 11, where an excitation with a frequency equal to half of the first linear natural frequency was applied. Although an excitation with very large amplitude was applied (50 000 N m^{-1}), the vibration displacement is not very large.

To have a first idea of the consequences of the Bauschinger effect on the dynamics of beams, the test with an excitation of 10 000 N m^{-1} at the linear fundamental frequency is repeated, but taking $M = 0.8$ (a value

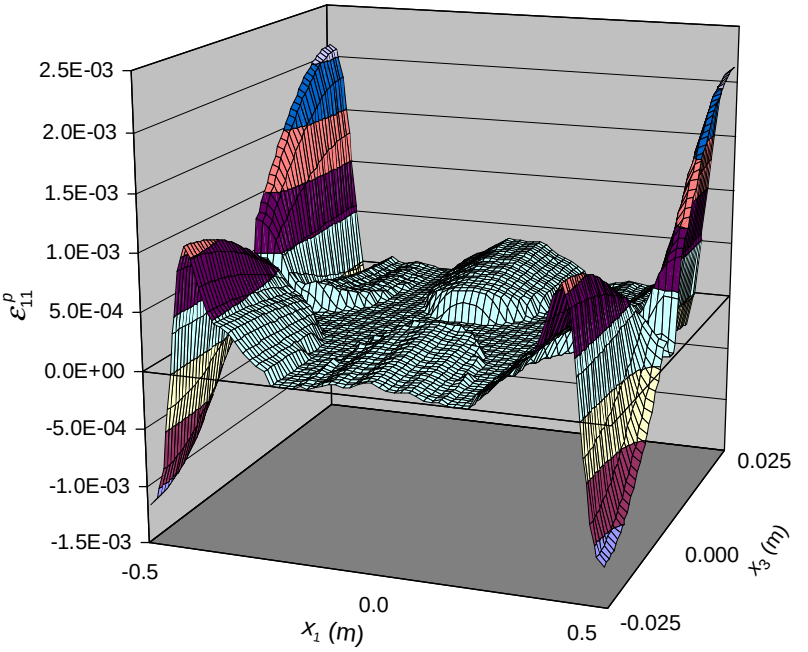

Fig. 10. Plastic strains $\varepsilon_{11}^{p}(x_1, x_3, t)$ at $t = 2.66736\,\mathrm{s}$ ($t/T_e = 682.913$), thick beam, excitation at linear natural frequency with $10\,000\,\mathrm{N\,m^{-1}}$ amplitude.

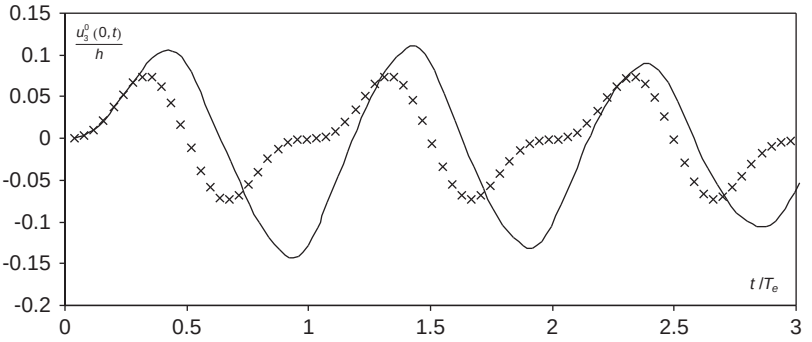

Fig. 11. (a) Transverse displacement of middle point, excitation at half the first linear natural frequency with $5 \times 10^4\,\mathrm{N\,m^{-1}}$ amplitude: — elasto-plastic and geometrically nonlinear; × geometrically nonlinear.

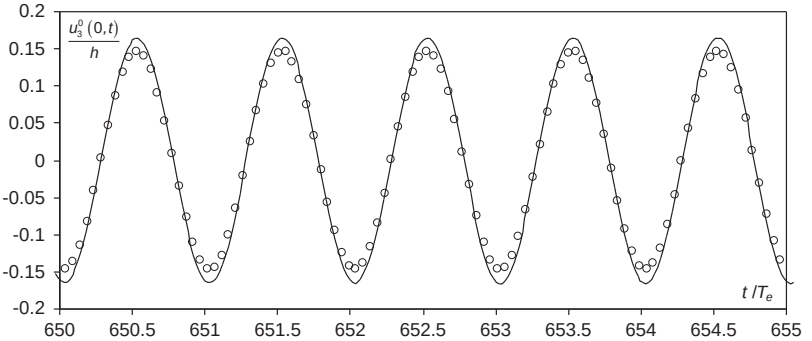

Fig. 12. Later cycles of transverse displacement of middle point of thick beam, excitation at linear natural frequency with $10\,000\,\mathrm{N\,m^{-1}}$ amplitude: — $M = 1$; ◦ $M = 0.8$.

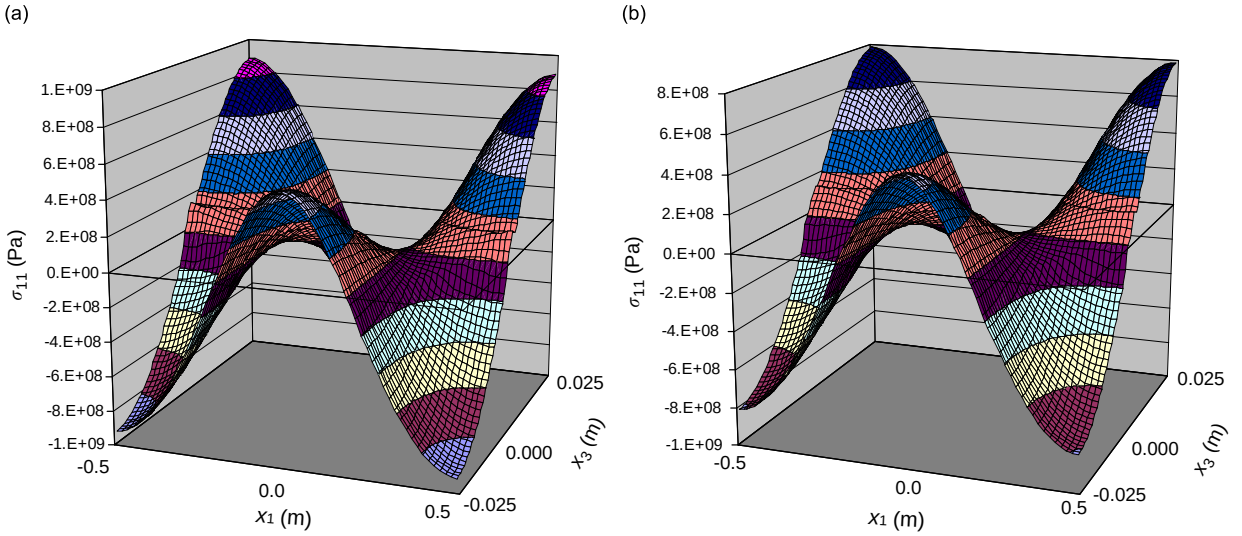

Fig. 13. Stresses $\sigma_{11}(x_1, x_3, t)$ at $t = 2.66736\,\mathrm{s}$ ($t/T_e = 682.913$), thick beam, excitation at linear natural frequency with $10\,000\,\mathrm{N\,m^{-1}}$ amplitude: (a) computed with $M = 1$; (b) computed with $M = 0.8$.

obtained from [6]) instead of $M = 1$, i.e., effectively using the Von Mises material model with mixed hardening that was presented in Section 2. Fig. 12 shows the transverse displacements between excitation cycles 650 and 655 computed with $M = 0.8$ and 1, both models elasto-plastic and geometrically nonlinear. Fig. 13 compares the stresses computed at $t = 2.66736\,\mathrm{s}$ ($t/T_e = 682.913$) without (Fig. 13(a)) and with (Fig. 13(b)) consideration of the Bauschinger effect.

The Bauschinger effect led to different evolution and distribution of plastic strains that had consequences in displacements and stresses. When the Bauschinger effect is included, the displacements slowly but steadily increase until, at least, the 700th cycle, where the computation was stopped. Steady state was not achieved. The plastic strains are, at the stage shown in the figures, changing much more significantly than if the Bauschinger effect is neglected. This probably means that the plastic work—which requires energy—is larger when the Bauschinger effect is considered because the yield surface changes locus. For this reason, the transverse displacements are smaller at the stage shown in the figures when computed with the Bauschinger effect, and consequently so are the total strains and stresses.

4. Conclusions

A method was proposed for dynamic analysis of beams, with consideration of plastic strains and geometrically nonlinear terms. The procedure is based on the *p*-version FEM and the stresses are computed following the governing parameter method. To investigate the robustness of the proposed approach, different parameters were tried in numerical tests and compared either with published data or with results computed using ANSYS. The element and procedure here suggested appear to be robust and able to provide accurate results. The main advantages of the beam *p*-version, hierarchical, element are that it requires fewer dof than *h*-version beam and shell elements, and provides a more detailed description of stress and strain fields than the *h*-version beam elements.

Plasticity was found to occur in a thin beam ($h/L = 0.01$) vibrating with displacement amplitude around its thickness; in a thicker beam plasticity occurred at relatively lower amplitudes. The appearance of plasticity can significantly change the dynamic behaviour of beams. In the first cycles of excitation, at the beginning of the transient phase, plastic zones develop that absorb energy and, therefore, the displacements can be significantly over predicted by models that solely consider geometrical nonlinearity. Once the plastic strains are established they are permanent and obviously interfere in the beam dynamics; the way in which they do that will depend

on the previous history of the motion and loading. With a periodic load, the fact that the combined plasticity and geometrical nonlinearity change the stiffness, and therefore the natural frequencies, may be significant in the dynamics of the beam.

Naturally, when plasticity occurs the stresses are influenced by it. If enough integration points are used, the *p*-version beam element provides depictions of the stress distribution with a detail comparable to *h*-version shell finite element models. It was found that under cyclic loading the stresses in zones where plasticity occurs can become somewhat irregular. This was particularly important near clamped boundaries and may require the use if quite high-order shape functions for a detailed description.

A first assessment of the Bauschinger effect on beam dynamics was made by carrying out tests on a thick beam. In the test shown, the Bauschinger effect led to smaller plastic strains but which changed more significantly and during more cycles than when the effect is neglected. As a consequence, energy dissipation due to plastic work increased and smaller displacements, as well as smaller total strains and stresses occurred.

Acknowledgement

The first author acknowledges the sabbatical scholarship SFRH/BSAB/582/2006 from Fundação para a Ciência e a Tecnologia, Portugal.

References

[1] R. Benamar, M.M.K. Bennouna, R.G. White, The effects of large vibration amplitudes on the mode shapes and natural frequencies of thin elastic structures—part I: simply supported and clamped–clamped beams, *Journal of Sound and Vibration* 149 (1991) 179–195.
[2] H. Wolfe, An Experimental Investigation of Nonlinear Behaviour of Beams and Plates Excited to High Levels of Dynamic Response, PhD Thesis, University of Southampton, 1995.
[3] P. Ribeiro, M. Petyt, Non-linear vibration of beams with internal resonance by the hierarchical finite element method, *Journal of Sound and Vibration* 224 (1999) 591–624.
[4] P. Ribeiro, A *p*-version, first order shear deformation, finite element for geometrically non-linear vibration of curved beams, *International Journal for Numerical Methods in Engineering* 61 (2004) 2696–2715.
[5] G.E. Dieter, *Mechanical Metallurgy*, McGraw-Hill, New York, 1986.
[6] M. Kojić, K.-J. Bathe, *Inelastic Analysis of Solids and Structures*, Springer, Berlin, 2005.
[7] J.-Y. Lee, P.S. Symonds, G. Borino, Chaotic responses of a two-degree-of freedom elastic–plastic beam model to short pulse loading, *Transactions of the ASME, Journal of Applied Mechanics* 59 (1992) 711–721.
[8] E. Manoach, D. Karagiozova, Dynamic response of thick elastic–plastic beams, *International Journal of Mechanical Sciences* 35 (1993) 909–919.
[9] U. Lepik, Elastic–plastic vibrations of a buckled beam, *International Journal of Non-Linear Mechanics* 30 (1995) 129–139.
[10] J.-X. Xu, N. Hasebe, The problem of an elastic–plastic beam dynamics and an incomplete co-dimension two bifurcation, *International Journal of Non-Linear Mechanics* 32 (1997) 127–143.
[11] R.P.S. Han, J. Lu, A space–time finite element method for elasto-plastic shock dynamics, *Journal of Sound and Vibration* 222 (1999) 65–84.
[12] J. Gerstmayr, H.J. Holl, H. Irschik, Development of plasticity and damage in vibrating structural elements performing guided rigid-body motions, *Archive of Applied Mechanics* 71 (2001) 135–145.
[13] J. Gerstmayr, H. Irschik, Vibrations of the elasto-plastic pendulum, *International Journal of Non-Linear Mechanics* 38 (2003) 111–122.
[14] G.W. Ma, Y.M. Liu, J. Zhao, Q.M. Li, Dynamic asymmetrical Instability of elastic–plastic beams, *International Journal of Mechanical Sciences* 47 (2005) 43–62.
[15] L. Meirovitch, H. Baruh, On the inclusion principle for the hierarchical finite element method, *International Journal for Numerical Methods in Engineering* 19 (1983) 281–291.
[16] A. Düster, E. Rank, The p-version of the FEM compared to an adaptive *h*-version for the deformation theory of plasticity, *Computer Methods in Applied Mechanics and Engineering* 190 (2001) 1925–1935.
[17] C.-Y. Chia, *Nonlinear Analysis of Plates*, McGraw-Hill, USA, 1980.
[18] T. Kaneko, On Timoshenko's correction for shear in vibrating beams, *Journal of Physics D* 8 (1975) 1927–1936.
[19] M. Abramowitz, I.A. Stegun (Eds.), *Handbook of Mathematical Functions with Formulas, Graphs, and Mathematical Tables*, National Bureau of Standards Applied Mathematics Series, Vol. 55, 1972.
[21] M.I. McEwan, J.R. Wright, J.E. Cooper, A.Y.T. Leung, A combined modal/finite element analysis technique for the dynamic response of a non-linear beam to harmonic excitation, *Journal of Sound and Vibration* 243 (2001) 601–624.
[22] K.J. Bathe, *Finite Element Procedures*, Prentice-Hall, Englewood Cliffs, NJ, 1996.
[23] S.G. Kelly, *Mechanical Vibrations*, McGraw-Hill, Singapore, 1993.